Nonperturbative Study of Thermonuclear Alfvén Instabilities in Next Step Burning Plasma Experiment.

N. N. Gorelenkov, R. Budny, C. Z. Cheng, G.-Y. Fu

C. Kessel, D. Meade, R. Nazikian

Princeton Plasma Physics Laboratory

P.O. Box 451, Princeton, NJ 08543-0451

H. Berk

IFS, Austin, Texas.

and

W.W. Heidbrink

University of California, Irvine, California 92697

ABSTRACT

A variaty of plasma conditions covering three major concepts of next step burning plasma experiment, ITER, FIRE and INGNITOR, are investigated against the stability of shear Alfvén eigenmodes. Main concern for such modes is the possibility of inflicting enhanced α-paricle losses to the first wall due to the instabilities driven by α-paricle pressure gradient. JET plasma, where fusion alphas were generated in tritium experiments, is included in the study for experimental validation of numerical predictions. High-n STability code HINST is the main used numerical tool, which is capable to predict instabilities of low frequency modes such as ballooning and Alfvén modes. HINST computes nonperturbative solutions of Alfvén eigenmodes including such effects as ion finite Larmor radius, orbit width, trapped electrons etc.. We show that towards large tokamaks such as International Thermonuclear Experimental Reactor (ITER) [*Plasma Physics and Controlled Nuclear Fusion Research* (International Atomic Energy Agency, Vienna, 1991), Vol. 3, p. 239] the spectrum of unstable AE modes, TAEs in particular, is shifted to medium-/high-n modes. TAEs are unstable locally due to alphas pressure gradient in almost all the devices under the consideration. However, NBI ions may produce strong stabilizing effect in plasmas like JET.

I. INTRODUCTION

Collective effects, such as instabilities driven by fast fusion products, alpha-particles, in the burning plasma experiments are critical physics issues for (i) the sustainment of the plasma parameters close to the ignition and (ii) for the heat fluxes to the first wall of the reactor. Collective effects are known to result in energetic particle transport and losses in the present day experiments. However, some plasma parameters of the burning plasmas can not be achieved in present devices. There are specific physical issues, which only arise at dimensionless plasma parameters relevant to next step burning plasma experiments (BP). In addition alpha particles will have close to isotropic distribution function, which distinguish BP from present day (PD) experiments. This affects the drive for known instabilities in the

plasma, such as Alfvén eigenmodes, fish-bones, and MHD macro-modes. Other important issue relavant to BP is the interaction of alphas with multiple Alfvén instabilities, which are difficult to achieve in PDs. Even with continued progress in PD experiments extrapolation to BP conditions may remain uncertain without BP experiment.

It is now generally acknowledged that Toroidal Alfvèn Eigenmodes [1–4] (TAE) destabilized by fast ions could cause significant difficulties for fusion ignition devices because of their capacity to induce large losses of fast particles. Even though TAE may play some positive role in burning tokamak-reactor plasma by means of providing a channel for fusion energy transfer to the plasma ions and He ash removal, the main concern here is that TAE induced losses could not only quench the ignition but also could lead to significant damage to the first wall. Previous low- to medium-n TAE instability studies indicated that fast particle drive $\gamma/\omega \sim n\beta_h(\rho_h/L_h)$, where n is the toroidal mode number, ρ_h is the fast ion Larmor radius, L_h is the fast ion pressure profile scale length, β_h is the fast ion thermal to magnetic pressure ratio. The fast particle drive reaches a maximum in n number near $nq^2\rho_h/r \simeq 1$ and decreases with increasing n for $nq^2\rho_h/r > 1$. On the other hand, the radiative damping rate of TAE due to core ion finite Larmor radius (FLR) effects increases with $k_\perp\rho_i$ [5, 6] at $k_\perp\rho_i > 1$, where $k_\perp$ is the characteristic perpendicular wavelength of TAE and ρ_i is the bulk ion Larmor radius calculated for ions with thermal velocity $v_T = \sqrt{2T/m}$. Thus, it is expected that in large scale fusion devices such as International Thermonuclear Experimental Reactor (ITER)[7], where $\rho_{h,i}/L_h \ll 1$, medium- to high-n TAE modes can be potentially unstable. It is therefore an urgent research need for the next step tokamak projects to study the medium- to high-n TAE mode stability, which requires numerical calculations.

The physics requirements for such high-n TAE stability code are discussed in Ref.[6] and have been incorporated into the HINST (high-n toroidal stability) code [8]. First, the code is able to treat non-ideal effects non-perturbatively. There are indications that non-ideal effects such as ion FLR effects and fast ion drive can strongly influence not only the growth rate but also the eigenfrequency, the eigenmode structure, and the existence of some TAE branches, like Resonant TAE (RTAE) [6] or Energetic Particle Modes (EPM) [9, 10]. Such

modes may be related to experimentally observed Beam Driven Eigenmodes (BAE) [11–13]. Secondly, the HINST code is able to reproduce many other TAE branches, like kinetic TAE (KTAE) and non-circularity induced TAE (NAE). Damping mechanisms including radiative, collisional and resonant damping on plasma species are considered. Also, fast particle drive is calculated with FLR effects and finite radial drift orbit width (FOW) effects. Among many AEs TAEs seems to be the most dangerous because of (i) their broad structure, which depends on the safety factor profile and typically on the order of $\sim \epsilon a$, (ii) spatial pressure gradient drive, and (iii) many modes can overlap radially and in the phase space.

II. MODEL OUTLINE

A. Fast particle TAE drive.

To understand the parametric dependence of the drive of TAE modes we make use of simplified expression for fast particles driven growth rate. Assume that fast particles have slowing down distribution funcion. Then as was shown in Ref. [14] the following expression for the growth rate can be obtained:

$$\begin{aligned} \frac{\gamma}{\omega} &= -\frac{3q^2\pi\beta_\alpha}{4}x_A\left\{\left[1+x_A\left(1-x_A\right)\right]-\frac{5}{18}\left[1+x_A^2\left(6-4x_A-3x_A^2\right)\right]\frac{\omega_*}{\omega}\right\}, \\ \frac{\omega_*}{\omega} &= -nq^2R\frac{2\rho_\alpha}{3x_Ar}\frac{\partial\ln\beta_\alpha}{\partial r}, \end{aligned} \tag{1}$$

where $x_A = v_A/v_{\alpha 0}$. As we mentioned above characteristic toroidal mode numbers for a given device are determined by fast particle orbit width:

$$n_{max} \simeq \frac{r}{q^2\rho_\alpha}. \tag{2}$$

From Eqs.(1,2) maximum expected growth rate is on the order:

$$\frac{\gamma_{\alpha max}}{\omega} \simeq -\frac{q^2R}{2}\frac{\partial\beta_\alpha}{\partial r}, \tag{3}$$

where we neglected terms with x_A. This expression may overestimate the growth rate since the FLR and FOW effects are not properly included. However the parametric dependence seems to be correct.

B. Damping and critical $\alpha-$particle pressure.

The damping rate dependence on plasma parameters is more complicated and includes TAE energy radiation through the thermal ion FLR effects and the modification of the eigenfunction. It can be expressed analytically only in limited domain of plasma parameters [14, 17], which will be used later in the paper for the comparison with numerical results. Nevertheless reasonable estimate of the damping, as we will see below in Sec.III A, can be obtained by including the dominant mechanism, thermal ion Landau damping. Analytical formula for Landau damping of Maxwellian ions[4] is applicable in the large aspect ratio limit for localized TAE solutions, such as core localized TAEs:

$$\frac{\gamma_d}{\omega} = \frac{q^2\sqrt{\pi}\beta_{pc}}{2} x_i^6 e^{-x_i^2} \tag{4}$$

where $x_i = v_A/3v_i \simeq \sqrt{2/9\beta_{pc}}$, thermal ion plus electron beta is plasma core beta β_{pc}, ion thermal velocity is $v_i = \sqrt{2T_i/m_i}$, and we assumed $x_i \gg 1$. Note, that this formula was shown numerically[18] to describe well the Landau ion damping for core localized TAEs.

Comparing the drive, Eq.(3), and the damping, Eq.(4) one can obtain the formula for the critical beta of hot particles:

$$\beta_{\alpha cr} = \frac{8}{3^6\beta_{pc}^2}\left(\frac{-R\partial \ln \beta_\alpha}{\partial r}\right)^{-1} e^{-2/9\beta_{pc}}. \tag{5}$$

We can include some dependence for the stability boundary in T and β_{pc} space as was suggested by Herb.

C. HINST kinetic nonperturbative numerical model

We use the nonperturbative fully kinetic code HINST[8]. HINST is able to reproduce RTAE branches with arbitrary drive. It includes bulk plasma and fast particle Finite Larmor Radius (FLR) effects. Radiative damping supported by trapped electron collisional effects and ion Landau damping. It has been improved (to be reported elsewere) to account for finite orbit width effects, numerical equilibrium, and other kinetic effects, such as nonadiabatic trapped electrons. Even though HINST is able to reproduce solutions with high toroidal n numbers that have radially localized mode structures, it can be used for medium-n to low-n modes in the local version of the HINST without resolving two-dimensional ($2D$) structure.

HINST was benchmarked against NOVA-K code for the case of strongly localized TAE modes: core localized TAEs. It shows agreement of the growth rate calculations between two codes within less than 20%. In section III A we compare HINST with analytical damping rates.

III. HINST MODELING OF TAE INSTABILITY

In this section we explore the stability of TAE modes in four different plasmas under the consideration, basing on modelilng of the tokamak analyzing code TRANSP[19]. Figure 1 shows cross sections of these devices. There is noticeable difference in dimensions of these tokamaks which parameters are shown in table I.

A. Fusion Ignition Research Experiment (FIRE)

We study this machine in more details. Figure shows comparison of TAE damping rates produced by HINST code without fast particle drive with analytical damping rates. Analytical expression for the damping includes ion Landau and radiative damping[14, 17]. The dependences are given as functions of minor radius variable $\sqrt{\Phi}$, where Φ is the toroidal

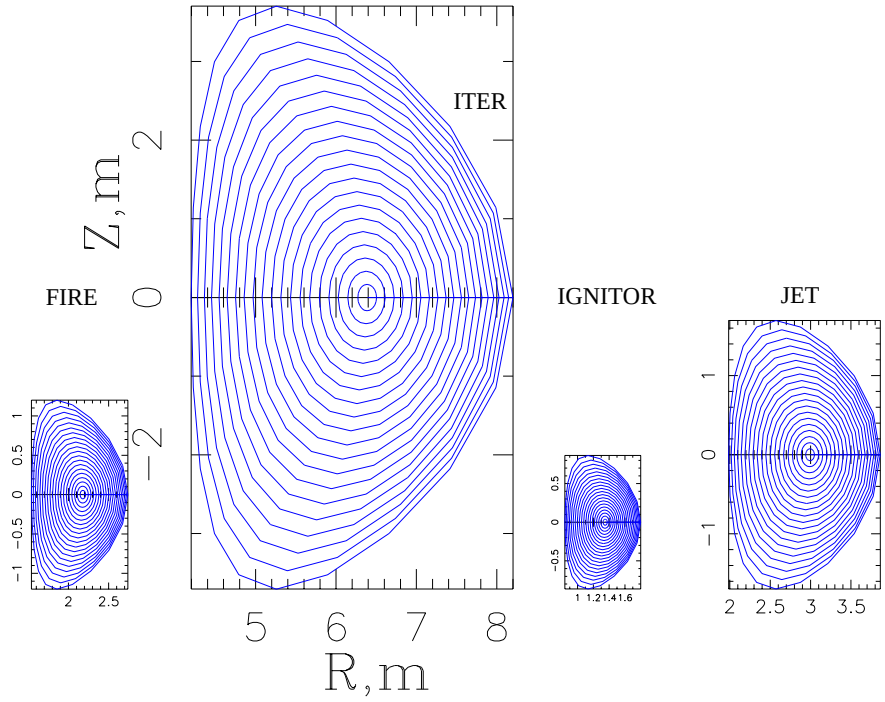

Figure 1: Plasma poloidal cross sections with magnetic surfaces of four tokamaks under the investigation: FIRE, ITER, IGNITOR, and JET. Relative sizes of these machines are compared as shown.

magnetic field flux. Numerical damping rates include radiative damping supported by thermal ion Landau and trapped electron collisional damping mechanisms. HINST code has reasonable agreement with the analytical formula within $0.35 < \sqrt{\Phi} < 0.5$, where the analytical formula can be applied. Closer to the edge, $\sqrt{\Phi} > 0.5$, trapped electron collisional damping is the strongest damping mechanism which contributes to the discrepancy, since the temperature decreases and the collsional frequency increases with minor radius. In the instability region ion Landau and trapped electron collisional damping are typically two competing mechanisms. Near the plasma center the frequency of core localized TAE approaches lower continuum and the analytical formula for the radiative damping is not valid. Note that the analytical ion Landau damping is within a factor of two from the HINST calculated damping and may be a good approximation for the total damping as we used

Tokamak	R,m	a,m	B_0, T	$\bar{n}, 10^{14} cm^{-3}$	$\beta(0)_\alpha, \%$	$-R\nabla\beta_\alpha, \%$	v_f/v_A	$v_A, 10^9 cm/sec$
ITER-FEAT	6.2	2	5.3	1	0.8	4	1.78	0.73
FIRE	2.14	0.6	10	4.9	0.31	1.5	1.79	0.725
IGNITOR	1.32	0.48	13.5	15.7	0.2	0.8	2.76	0.47
JET-DT	2.92	0.94	3.82	0.45	0.4	2.3	1.65	0.785

Table I: Main plasma parameters for tokamaks under the consideration.

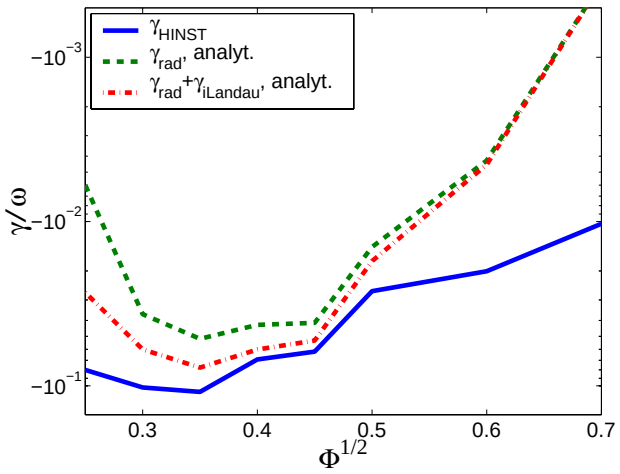

Figure 2: Comparison of numerical damping rates from HINST code with the analytical ones in FIRE for $n = 10$ TAE.

above.

For the instability calculations we use TRANSP computed plasma core and α-particle beta profiles shown on figure 3 .

Results of HINST code for FIRE plasma are shown in figure 4 in the form of the eigenfrequency and the growth rate for TAEs as functions of $\sqrt{\Phi}$.

Figure 5 shows the eigenfrequency and the growth rate computed by local HINST code versus TAE toroidal mode number. We are showing the dependence of HINST calculated

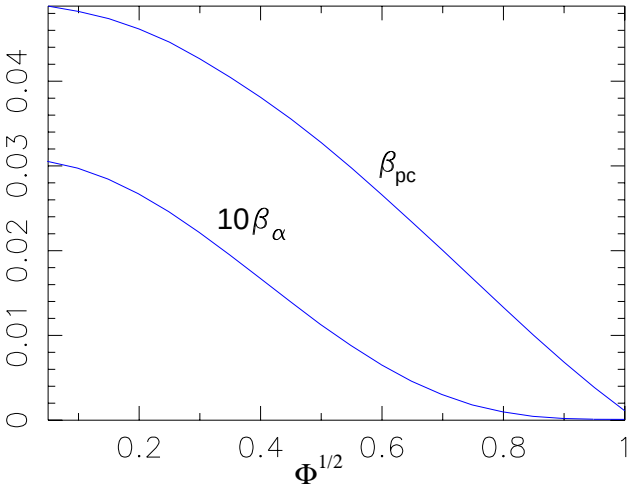

Figure 3: Plasma core and alpha particle pressure as functions of the minor radius variable $\sqrt{\Phi}$ in FIRE.

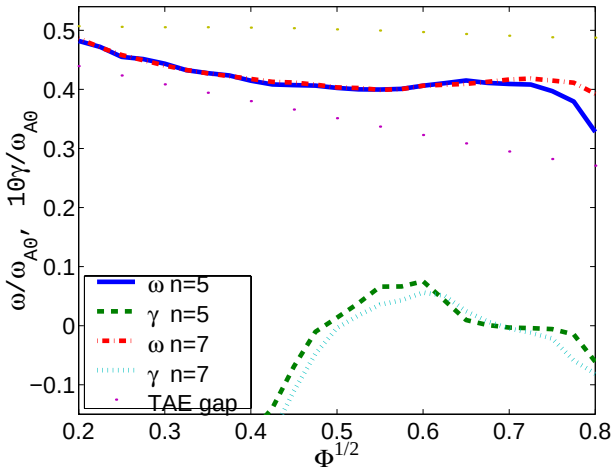

Figure 4: TAE eigenfrequency and growth rate as a function of the minor radius variable $\sqrt{\Phi}$ in FIRE.

TAE instability critical beta of $\alpha-$particles in figure 6 on minor radius. Note that with TRANSP calculated value of $\beta_\alpha(0) = 0.31\%$ TAE unstable region spanns within $0.5 < \sqrt{\Phi} < 0.65$ and sharply increases outside. TAEs are the modes which radial width depends on the shape of the continuum gap and is typically broad. Since the global solution of TAE

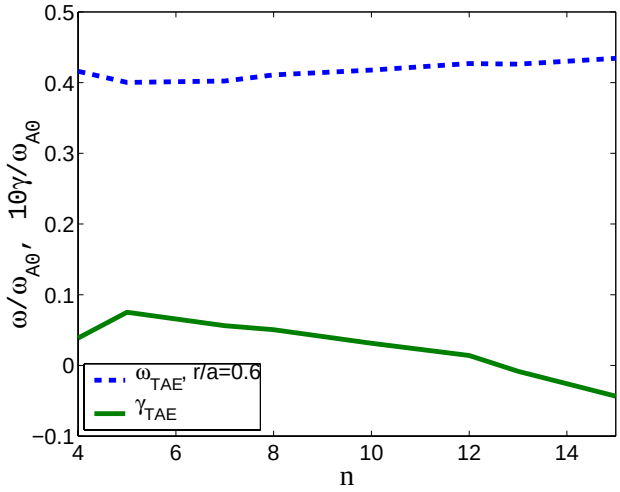

Figure 5: Eigenfrequency and growth rate of TAE vs. toroidal mode number as computed by HINST in FIRE.

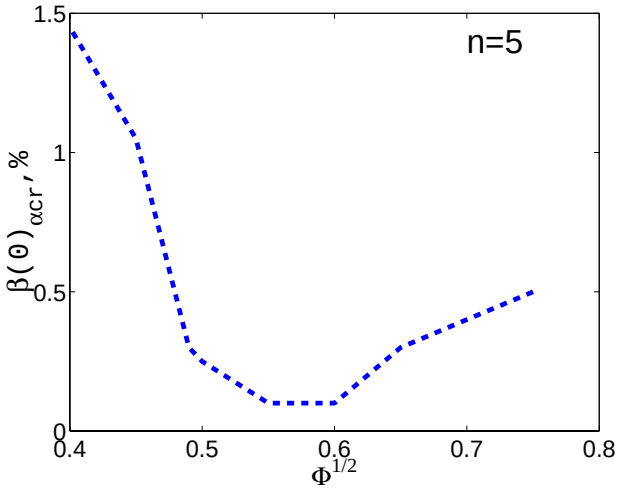

Figure 6: TAE instability α-particle critical betas in FIRE.

needs averaging over large portion of minor radius the final question of TAE critical beta will require global calculations. Such effect as stronger mode coupling through plasma shaping may introduce stronger continuum damping [20].

B. International Tokamak Experimental Reactor (ITER)

We perform similar TAE instability growth rate calculations for ITER. Figure 7 shows

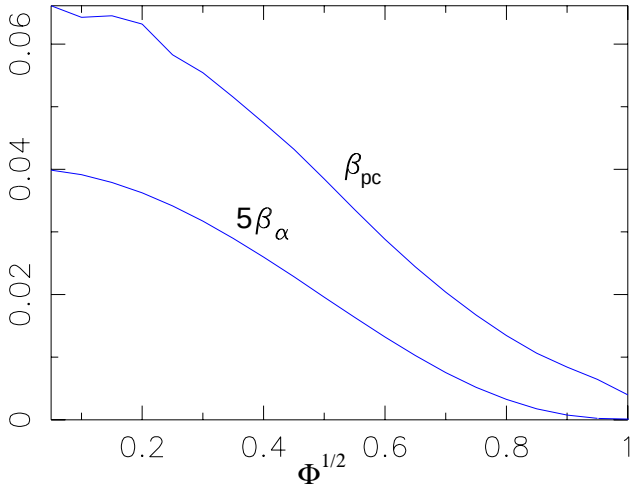

Figure 7: Plasma core and alpha particle pressure as functions of the minor radius variable $\sqrt{\Phi}$ in ITER.

radial profiles of the background plasma and α-particle beta.

TRANSP predicted safety factor profile is shown on Fig.8. Numerical q-profile is not monotonic due to several factors, such as NBI and ICRH heating used in TRANSP. We are performing the sensitivity study of TAE instability to the shape of q-profile with the smoothed q-profile according to the formula $q = 1 + 2.8\Phi^{3/2}$.

Figures 9 and 10 epresent the eigenfrequency and the growth rate computed by HINST code of TAE as functions $\sqrt{\Phi}$ and toroidal mode number n, respectively. As expected from our estimates in table I maximum growth rate for ITER ar least in local calculation is shifted to higher $n \simeq 9$. Nonetheless the total number of ustable mode is about the same.

In ITER there are plans to use high energy NBI heating. This may contribute to the drive or damping of TAEs depending on energy of beam ions. Figure 11 shows the contribution of NBI fast ions as a function of their birth energy at the point of maximum α-particle growth rate $\sqrt{\Phi} = 0.5$. Expected injection energy of NBI ions is $1MeV$. From our calculations it

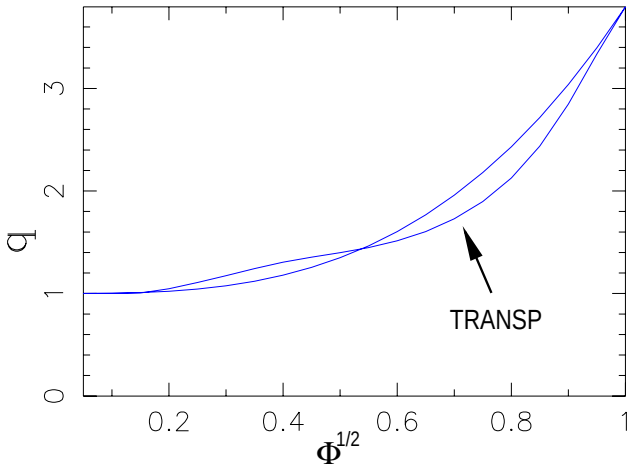

Figure 8: q-profile as calculated by TRANSP and smoothed q-profile to study its effect on TAE stability.

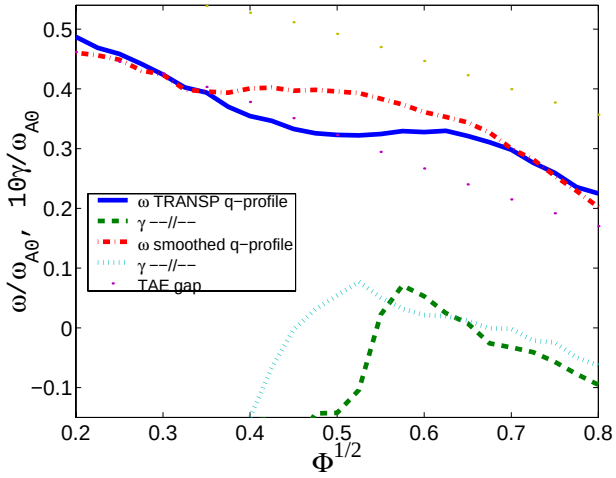

Figure 9: TAE eigenfrequency and growth rate as functions of the minor radius variable $\sqrt{\Phi}$ in ITER.

follows that the energy of NBI ions may be reduced to achieve the stabilization of TAEs. This may provide a control to TAE stability.

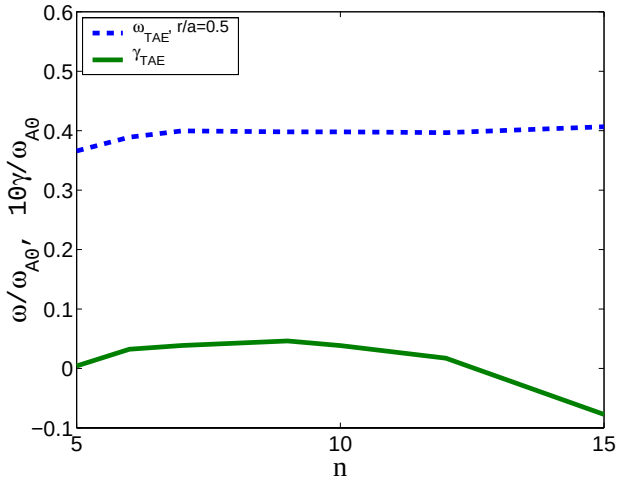

Figure 10: Eigenfrequency and growth rate of TAE vs. n as computed by HINST in ITER.

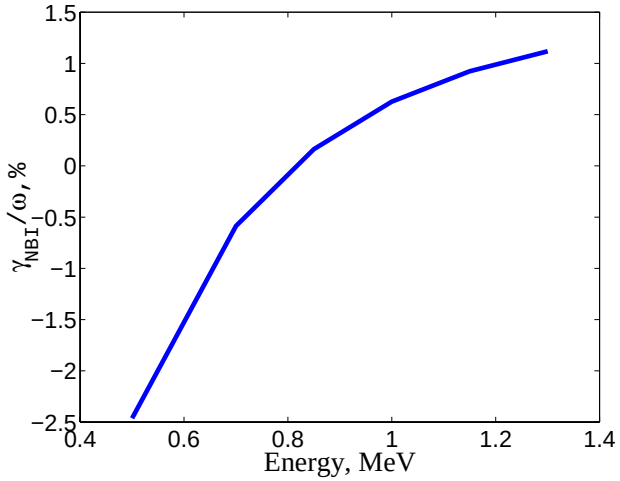

Figure 11: Contribution of NBI ions to the growth rate of TAE as a function of the injection energy in ITER at $\sqrt{\Phi} = 0.5$.

C. IGNITOR

Figure 12 presents the background core plasma and α-particle beta profiles as functions of $\sqrt{\Phi}$.

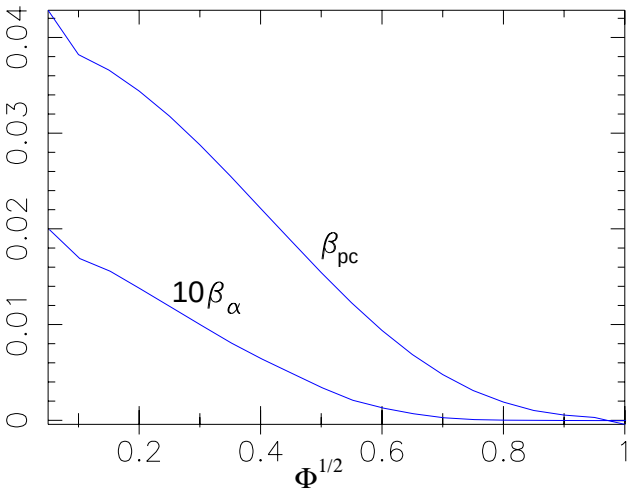

Figure 12: Background core plasma and alpha particle beta as functions of the minor radius variable $\sqrt{\Phi}$ in IGNITOR.

Figure 13 represents the eigenfrequency and the growth rate of TAE functions of $\sqrt{\Phi}$.

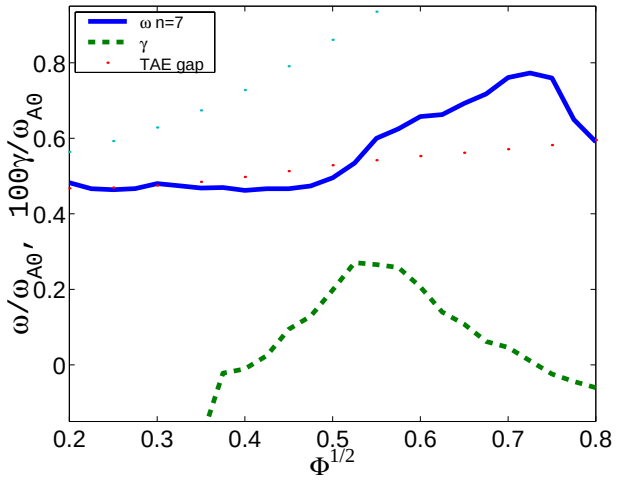

Figure 13: TAE eigenfrequency and growth rate as functions of the minor radius variable $\sqrt{\Phi}$ in IGNITOR.

Figure 14 shows the eigenfrequency and the growth rate computed by local HINST code and their dependence on the toroidal mode number.

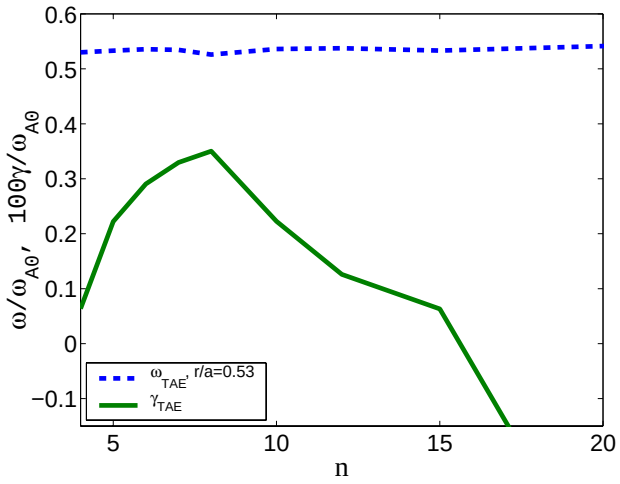

Figure 14: Eigenfrequency and growth rate of TAE vs. n as computed by HINST in IGNITOR.

D. JET

Figure 15 presents the background core plasma and α-particle beta profiles as functions

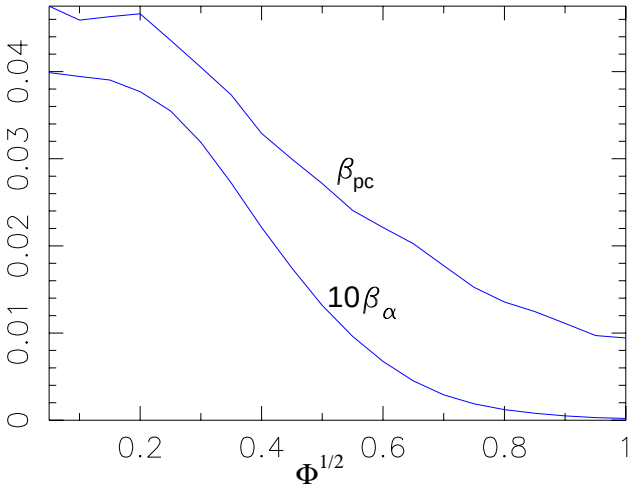

Figure 15: Background core plasma and alpha particle beta as functions of the minor radius variable $\sqrt{\Phi}$ in JET.

of $\sqrt{\Phi}$.

Figure 13 represents the eigenfrequency and the growth rate of TAE as functions of $\sqrt{\Phi}$.

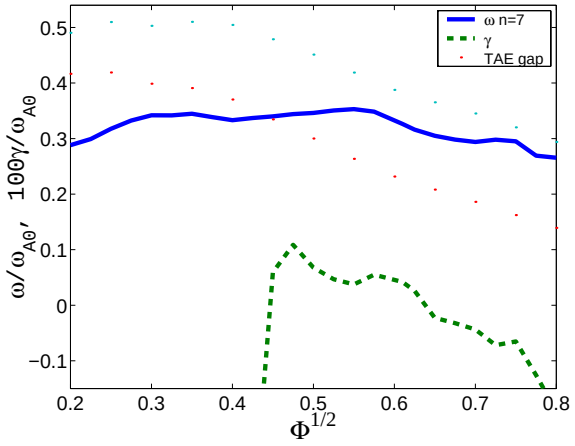

Figure 16: TAE eigenfrequency and growth rate as functions of the minor radius variable $\sqrt{\Phi}$ in JET.

Figure 14 shows the eigenfrequency and the growth rate computed by HINST code and their dependence on the toroidal mode number. In JET nonmonotonic behavior of growth

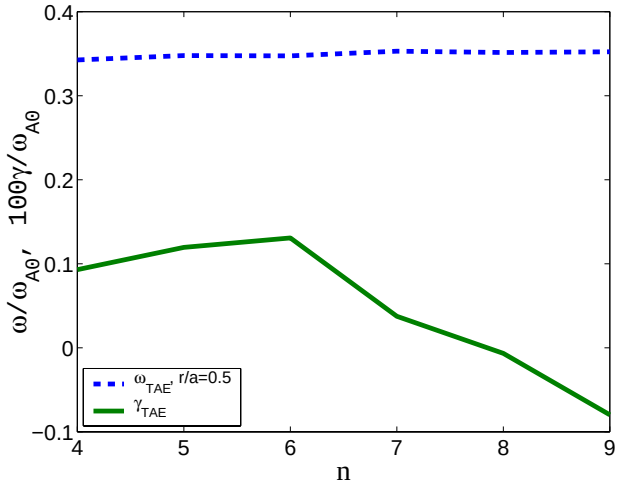

Figure 17: Eigenfrequency and growth rate of TAE vs. n as computed by HINST in JET.

rate dependence on the radius is due to used numerical betas of plasma and α-particles. The

maximum growth rate in JET is lower and is expected to be at $n \simeq 6$, which close to what was predicted in other studies [21, 22]. Nevertheless used NBI heating provides stabilizing effect. We computed TAE growth rate for NBI beta $\beta_b(0) = 0.6\%$ at injection energy of deuterium $\mathcal{E}_{b0} = 100keV$. HINST shows large damping rate due to NBI ions $\gamma/\omega \simeq 5\%$. As was expected in JET the number of unstable mode is small $n \leq 7$.

---

[1] C. Z. Cheng, L. Chen, M. S. Chance, Ann Phys. (NY) **161**, 21 (1985).

[2] C. Z. Cheng and M. S. Chance, Phys. Fluids **29**, 3695 (1986).

[3] C. Z. Cheng, G. Y. Fu, and J. W. Van Dam, Princeton Plasma Physics Laboratory Report, PPPL-2585 (January, 1989), 14pp. *in Proceedings of the Joint Varrena-Lausanne Workshop on Theory of Fusion Plasmas,* Lausanne, Switzerland, Oct. 3-7, 1988, p. 259-270.

[4] G. Y. Fu and J. W. Van Dam, Phys. Fluids B **1**, 1949 (1989).

[5] R. R. Mett and S. M. Mahajan, Phys. Fluids B **4**, 2885 (1992).

[6] C. Z. Cheng, N. N. Gorelenkov, and C. T. Hsu, Nucl. Fusion **35**, 1639 (1995).

[7] *Plasma Physics and Controlled Nuclear Fusion Research* (International Atomic Energy Agency, Vienna, 1991), Vol. 3, p. 239.

[8] N. N. Gorelenkov, C. Z. Cheng, and W. M. Tang, Phys. Plasmas **5**, 3389 (1998).

[9] L. Chen, Phys. Plasmas **1**, 1519 (1994).

[10] R. A. Santoro and L. Chen, Phys. Plasmas **3**, 2349 (1996).

[11] W. W. Heidbrink, E. J. Strait, E. Doyle, G. Sager, and R. Snider, Nucl. Fusion **31**, 1635 (1991).

[12] W. W. Heidbrink, E. J. Strait, M. S. Chu, and A. D. Turnbull, Phys. Rev. Lett. **71**, 855 (1993).

[13] N. N. Gorelenkov and W. W. Heidbrink, Nucl. Fusion **42** (2002).

[14] H. L. Berk, J. W. Van Dam, Z. Guo, and D. M. Lindenberg, Phys. Fluid B **4**, 1806 (1992).

[15] C. Z. Cheng, Phys. Fluid B **3**, (1991).

[16] H. L. Berk, R. R. Mett, and D. M. Lindenberg, Phys. Fluid B **5**, 3969 (1993).

[17] G. Y. Fu, C. Z. Cheng, R. Budny, et.al., Phys. Plasmas **3**, 4036 (1996).

[18] N. N. Gorelenkov, Phys. Plasmas, (1999).??

[19] R. V. Budny, submitted to Nucl. Fusion **42**, (2002).

[20] A. Jaun, A. Fasoli, J. Vaclavik, L. Villard, Nucl. Fusion **40**, 1343 (2000).

[21] S. Sharapov, *et.al.,* Nucl. Fusion **39**, 373 (1999).

[22] D. Borba, *et.al.,* Nucl. Fusion **40**, 775 (2000).

R. V. Budny, Nucl. Fusion **34**, 1247 (1994).

The JT-60 Team, in *Plasma Physics and Controlled Nuclear Fusion Research*, Proceedings of the 14th International Conference, Würzburg (International Atomic Energy Agency, Vienna, 1993), Vol. I, p. 57.

J. W. Connor, R. J. Hastie, and J. B. Taylor, Proc. R. Soc London Ser. A **365**, 1 (1979).

F. Zonca, Ph.D. thesis, Princeton University, 1993.

F. Zonca and L. Chen, Phys. Fluids B **5**, 3668 (1993).

J. W. Connor, J. B. Taylor, and H. R. Wilson, Phys. Rev. Lett. **70**, 1803 (1993).

G. Vlad, et al., Nucl. Fusion **35**, 1651 (1995).

W. W. Heidbrink, E. J. Strait, E. Doyle, G. Sager, and R. Snider, Nucl. Fusion **31**, 1635 (1991).

W. W. Heidbrink, E. J. Strait, M. S. Chu, and A. D. Turnbull, Phys. Rev. Lett. **71**, 855 (1993).

R. L. Dewar, in *Theory of Fusion Plasmas*, edited by A. Bondeson, E. Sindoni, and F. Troyon (Soc. Ital. Fisica-Editrice Compositori, Belgium, 1988).

Y. Z. Zhang and S. M. Mahajan, Phys. Lett. A **157**, 133 (1991).

X. D. Zhang, Y. Z. Zhang, S. M. Mahajan, Phys. Fluid B **5**, 1257 (1993).

M. N. Rosenbluth, et al. Phys. Rev. Lett. A **68**, 596 (1992).

T. M. Antonsen and B. Lane, Phys. Fluids **23**, 1205 (1980).

P. J. Catto, et al., Plasma Phys., **23**, 639 (1981).

Mikhailovskii, A. B., in *Reviews of Plasma Physics*, edited by M. A. Leontovich (Consul-

tants Bureau, New York, 1986), Vol. 9, p. 103.

I. S. Gradshteyn and I. M. Ryzhik, *Table of Integrals, Series and Products.* Academic, San Diego, Calif., 1963.

C. Z. Cheng and M. S. Chance, J. Comput. Phys., **71**, 124-146 (1987).

R. L. Dewar, and A. H. Glasser, Phys. Fluid **26**, 3038 (1983).